Axial Disposition of Myosin Heads in Isometrically Contracting Muscles

J. Juanhuix,* J. Bordas,* J. Campmany,* A. Svensson,† M. L. Bassford,† and T. Narayanan‡

*Laboratori Llum Sincrotró-Institut Física Altes Energies, Universitat Autònoma de Barcelona, E-08193 Bellaterra, Barcelona, Spain; †Department of Physics and Astronomy, University of Leicester, Leicester LE1 7RH, United Kingdom; and ‡European Synchrotron Radiation Facility , F-38043 Grenoble, France

ABSTRACT Meridional x-ray diffraction diagrams, recorded with high angular resolution, from muscles contracting at the plateau of isometric tension show that the myosin diffraction orders are clusters of peaks. These clusters are due to pronounced interference effects between the myosin diffracting units on either side of the M-line. A theoretical analysis based on the polarity of the myosin (and actin) filaments shows that it is possible to extract phase information from which the axial disposition of the myosin heads can be determined. The results show that each head in a crown pair has a distinct structural disposition. It appears that only one of the heads in the pair stereospecifically interacts with the thin filament at any one time.

INTRODUCTION

The meridional part of the x-ray diffraction diagram of striated muscles is proportional to the square of the modulus of the Fourier transform of the mass projection of the structure onto the muscle axis. Therefore, and especially given the elongated shape of the S1 sub-fragment (Rayment et al., 1993), the meridional reflections on the myosin layer lines, following a sequence of orders of a repeat of ~43.0 nm at rest, are sensitive to the axial orientation of the myosin heads. For these reasons, the myosin meridional reflections, and in particular the strongest order on the third myosin layer line (3M) at a rest spacing of 14.34 nm, have been extensively used as markers for myosin head disposition during various forms of contraction, initially in whole muscles (Huxley et al., 1981, 1982, 1983) and more recently in muscle fibers (Irving et al., 1992; Dobbie et al., 1998). These experiments have been interpreted as providing supportive, but not conclusive, evidence for models of contraction based on axial swings of various parts of the myosin molecule coupled to the hydrolysis of ATP (Huxley, 1969, 1974; Holmes, 1997). Because the knowledge of the phases associated with the diffraction features have been up to date lacking, the interpretation of the data had to rely on modeling. The fact that there is a pair of heads in the double-headed myosin molecule adds an additional complication, and generally, data were interpreted assuming that both heads in the pair had the same axial orientation.

Here we present experimental results where the meridional diffraction features at the plateau of isometric tension (P_o) are recorded with the kind of angular resolution only achievable with third-generation synchrotron radiation (SR) sources. The data show that all the meridional reflections on the myosin layer lines, up to the 15th order (i.e., the 3M, 6M, 9M, and 15M, with the 12M being too weak to measure) are carved up by interference effects so that clusters of peaks appear on the meridional reflections due to the axial disposition of the heads. We show that with appropriate theoretical analysis of these effects one can extract phase information from which the axial distribution of the myosin heads can be determined. The results show that at P_o, each myosin head in the pair has a distinctly different axial orientation.

MATERIALS AND METHODS

Data collection and reduction

Two-dimensional x-ray diffraction patterns from frog sartorius muscles from *Rana esculenta* contracting isometrically at ~7°C were collected at P_o. The measurements were carried out at Beamline 4-ID2 at the European Synchrotron Radiation Facility (ESRF, Grenoble, France) using x-rays with a wavelength of 0.0989 nm. A description of this station has been given elsewhere (Boesecke et al., 1995).

Tetani of 800 ms were applied and patterns were recorded by opening a fast shutter when tension had reached P_o. Image plates were used as the x-ray-detecting medium. Rest patterns were also recorded for reference. Two different camera setups were used. In one set of experiments data collection was carried out in a range extending from ~500.0 to 4.2 nm using a 7-m camera such that meridional reflections above and below the direct beam could be recorded. Rest patterns were also recorded for calibration purposes. In this manner high precision in the determination of the absolute spacing could be achieved. The fast shutter was opened 200 ms after the onset of stimulation and kept open for 500 ms as the plateau of tension was maintained. Each muscle was discarded after one single exposure. Measurements were also carried out with a camera length of 9.775 m, in which the equator and only the top half of the two-dimensional patterns could be measured. In this case the shutter was opened 250 ms after stimulation and kept open for 500 ms. Three exposures per muscle, with a vertical muscle shift of 1 mm between exposures to avoid radiation damage, were used in these protocols. Both angular and real-space resolution (the resolution of the data could be extended to ~2.4 nm) was greatly improved with this procedure, but the diffraction origin had to be deduced from extrapolation of the equatorial reflections (10 and 11) on either side of the beam stop, rather than by the more direct approach of using meridional reflections above and below it. Absolute spacing was determined by assigning to the third myosin meridional reflection at rest a spacing of 14.34 nm. No difference in data quality, other than that expected

Received for publication 28 January 2000 and in final form 12 December 2000.

Address reprint requests to Dr. Joan Bordas, Edifici Ciencies Nord, LSB-IFAE, Campus UAB, E-08193 Bellaterra, Spain. Tel.: 34-93-581-28-54; Fax: 34-93-581-32-13; E-mail: jbordas@ifae.es.

0006-3495/01/03/1429/13 $2.00

for a longer camera length, could be detected with respect to the other protocol.

The stimulating protocols, the approach used to calibrate the image plate scanner for spatial nonlinearities, and the peak-stripping procedures employed to fit polynomials to the backgrounds and Gaussian functions to the diffraction maxima were all as described before (Bordas et al., 1999). The only constraint applied to the peak-stripping procedures was that the Gaussian widths of partly overlapping reflections were forced to be identical.

Function fits to the experimental data

The theoretical functions, used to fit the experimental traces, were calculated with the same grid as that of the experimental results, i.e., the nm^{-1}/pixel was the same. Experimental meridional traces were obtained by radial integration in the region comprised between -0.02 and 0.02 nm^{-1}. The parameters in the theoretical function whose value had to be refined to reproduce the experimental results, i.e., floating parameters in the minimization, were varied over a wide range and residuals R calculated as follows:

$$R^2 = \sum_{\mathrm{j}} \frac{[I(Z_\mathrm{j})_{\mathrm{exp}} - I(Z_\mathrm{j})_{\mathrm{calc}}]^2}{I(Z_\mathrm{j})^2_{\mathrm{exp}}},$$

where $I(Z_\mathrm{j})_{\mathrm{exp}}$ and $I(Z_\mathrm{j})_{\mathrm{calc}}$ are the experimentally determined intensity distribution and the calculated one at a given pixel j, respectively. Residuals were determined for the fit in each meridional order. After finding approximate values of the floating parameters for which the residuals went through a minimum, the fitting was refined by repeating the calculations with a finer grid. A point-spread function with a half-width at half-maximum of ~2.6 image plate pixels (equivalent to ~260 μm or ~2.7×10^{-4} nm^{-1}) was convoluted with the calculated function. This was to account for the camera focal spot size and image plate resolution in the direction of the muscle axis. No attempt was made to correct for arching of the layer lines.

Calculation of mass projections from the three-dimensional structure of pairs of myosin heads

Electron density maps corresponding to the mass projection of pairs of myosin heads onto the muscle axis were obtained from the atomic structure of the myosin head (Rayment et al., 1993). The atomic coordinates of the α-carbons in the polypeptide chain of myosin heads were translated so that the origin of a system of Cartesian coordinates was placed at the tip of the tail end. The heads were then aligned so that the y axis ran through their long axis. The z axis was assumed to be the muscle axis and onto which mass projections had to be calculated. The myosin heads were rotated around the y axis and inclined relative to the z axis by rotation around the x axis. Also, one head in the pair was translated along the z axis relative to the other. Thereafter, the mass projection onto the z axis was calculated by summing the density of the atoms with their x and y coordinates falling within an interval of 0.7 nm. The resolution of the calculated mass projection was brought approximately to the level of the experimental data by convoluting the calculated mass projection with a Gaussian function with a half-width at half-maximum of 0.6 nm. The resulting mass projection onto the z axis was then compared with the experimentally determined ones. Minimization between the calculated and experimentally determined mass projections was carried out using the same approach employed for function minimization.

RESULTS

Experimental

C-protein and troponin periodicities at rest and P_o

Meridional traces of x-ray patterns from resting muscles have diffraction features due to structures other than myosin heads (Huxley and Brown, 1967; Haselgrove, 1975; Rome, 1972; Malinchik and Lednev, 1992). In particular, diffraction peaks due to the C-protein and troponin periodicities, sampled by interference effects (Rome et al., 1973a,b), are clearly present. Their analysis has yielded repeat values of 43.5–44.2 nm and 38.5–38.8 nm for C-protein and troponin, respectively (Rome, 1972; Rome et al., 1973a,b; Squire, 1981). Given that myosin heads at P_o have a repeat of ~14.54 nm (see below) there is the possibility that C-protein may contribute to the meridional intensities in the region of the 3M, 6M, 9M, and 15M myosin meridional reflections. The behavior and analysis of these myosin features is the main concern of this report, and consequently, it is important to establish whether C-protein has a significant contribution to their intensities at P_o. In addition, as the eighth order of the troponin repeat falls close to the position of the 9M, the same considerations apply here.

C-protein and troponin features are clearly present at P_o, but they are much weaker than at rest. For example, the total integrated intensities of the clusters in the first orders of C-protein and troponin amount to ~1/10 and 1/4, respectively, of those at rest (Table 1). It would appear from the position and intensities of the peaks in these clusters (Table 1) that the C-protein repeat at P_o is somewhat longer than at rest. However, as there are many other weak reflections taking the appearance of a long-range beating effect, one cannot be certain that the positions and intensities of the interference maxima are not distorted. Therefore, we believe that a more precise estimate of the C-protein periodicity at P_o can be obtained from meridional clusters of higher orders, where cleaner diffraction features are present.

Specifically, the region of the fourth order of C-protein (4C) is a good candidate to determine more precisely the axial rise of C-protein at P_o. The 4M/4C region at rest consists of a cluster of peaks (Table 1). Given their spacing, one can assume with a fair degree of certainty that the peaks at 10.81 and 10.67 nm are mostly due to the fourth order of the axial rise of the myosin heads at rest sampled by a long-range interference effect. On the other hand the peaks at ~11.36, 11.17, and 10.96 nm have a spacing that is too long to be due to the myosin heads, and they must contain the expected contribution from a C-protein periodicity. At P_o the peaks attributable to the myosin heads disappear, and only two weak peaks at spacings of ~11.15 and 10.98 (whose total integrated intensity is ~10% of that at rest) are visible. This suggests that the disappearance of the myosin contribution at P_o leaves a cluster entirely due to C-protein. From the relative intensity of these two maxima (Table 1)

TABLE 1 Spacings and relative intensities

Order	Spacings (nm) and relative intensities at rest	Spacings (nm) and relative intensities at P_o	Relative total intensity in cluster (P_o/rest)
1M/1C	46.68 [0.10]	47.56 [0.26]	0.12
	44.17 [1.00]	44.66 [1.00]	
	41.38 [0.24]	43.44 [0.40]	
		41.14 [0.15]	
1T	39.45 [0.93]	39.28 [0.60]	0.25
	38.18 [1.00]	28.27 [1.00]	
3M/3C	15.44 [0.04]		0.50
	15.09 [0.03]	14.89 [0.02]	
	14.83 [0.03]	14.64 [1.00]	
	14.55 [0.06]	14.43 [0.82]	
	14.34 [1.00]	14.30 [0.10]	
	14.14 [0.18]	14.13 [0.05]	
4M/4C	11.17 [0.36]	11.14 [0.30]	0.10
	10.97 [0.40]	10.98 [1.00]	
	10.81 [0.08]		
	10.67 [1.00]		
6M/6C	7.43 [0.03]		0.69
	7.38 [0.02]		
	7.28 [0.02]	7.30 [1.00]	
	7.22 [0.07]	7.24 [0.49]	
	7.18 [1.00]	7.18 [0.11]	
	7.12 [0.64]		
9M/9C	4.90 [0.05]		2.04
	4.86 [0.52]	4.87 [0.31]	
8T	4.81 [0.66]	4.84 [1.00]	
	4.78 [1.00]		
	4.77 [0.09]		
	4.74 [0.32]		
15M	2.87 [1.00]	2.92 [0.19]	1.67
	2.86 [0.84]	2.91 [1.00]	

The first column identifies the potential contribution of different structures (C, C-protein; T, troponin; M, myosin) to the various clusters numbered with the order of the repeat. The second column is the approximate spacing of various peaks present in each cluster at rest. In brackets are the intensities of each peak in a given cluster relative to the most intense one, which is taken as unity. The third column presents the equivalent information for the data at P_o. Finally, the fourth column gives the relative total intensities between P_o and rest for each cluster.

and using the arguments previously applied to the low-angle reflections (Squire, 1981), one would conclude that the fourth order of C-protein at P_o is sampled by an interference distance of ~700 nm and that C-protein has a repeat of ~44.0 nm.

In regard to the troponin periodicity at P_o, we find that its first order is characterized by two peaks at spacings of ~39.28 and 38.25 nm, from whose relative intensities (1T, Table 1) and from previously developed arguments (Squire, 1981), one derives a troponin periodicity of ~38.7 nm. Similar values can be derived in the region of the 2T and 3T.

In summary, the limited amount of data presented here indicates that the C-protein and troponin periodicities at P_o are ~44.0 and 38.7 nm, respectively. In addition, their contribution to the diffraction pattern at P_o is much less prominent than at rest and, as we show below, practically negligible with respect to the 3M, 6M, 9M, and 15M intensities at P_o.

Comparison of meridional diffraction features at rest and P_o

Meridional traces at rest and P_o in the regions of the 3M, 6M, 9M, and 15M are compared in Fig. 1. For the purpose of comparison the traces at P_o have been scaled, after background subtraction, between a minimum value of zero and a maximum value of one for all clusters. Table 1 (third column) provides the relative integrated intensities for the various clusters.

There are several relevant points to note. 1) The center of gravity of all clusters moves to low angles by ~1.6% during the transition from rest to P_o. 2) The 3M, 6M, and 15M rest patterns show negligible intensity at the position of the peaks present in the P_o clusters. 3) The 9M cluster at rest consists of a number of peaks (Table 1). Those at spacings of ~4.90 and 4.86 nm (i.e., at ~0.2040 and 0.2058 nm^{-1}) may be attributed to the C-protein repeat sampled by an interference effect. A relatively intense peak at a spacing of ~4.81 nm (i.e., the peak at ~0.2077 nm^{-1}) is close to the position expected for the eighth order of the troponin repeat, and this is its likely origin. The overlapping peaks at spacings of ~4.78, 4.77, and 4.74 (i.e., at 0.209, 0.2099, and 0.2107 nm^{-1}) are at the positions expected from the ninth order of a rest spacing of $3 \times (14.31 - 14.32)$ nm sampled by an interference effect. We note in passing that the axial rise of the myosin heads at rest is somewhat shorter than 3×14.34 nm. This is because interference effects at rest do not sample the 3M at exactly the position of the center of the underlying Laue function. 4) The 9M cluster at P_o consists of two main peaks at a spacing of 4.84 and 4.87 nm. If the positions and the intensities of the rest peaks under the P_o cluster did not change during the transition from rest to P_o, their contribution to the 9M cluster at P_o would amount to <15%. Considering that the intensities of all the other C-protein/troponin clusters (Table 1) undergo a substantial decrease during the transition from rest to P_o, it is likely that their contribution to the 9M cluster is considerably less than 15%. 5) The high-angle side of the 9M trace at P_o has a weak shoulder that may be either an arching artifact or a remnant of the eighth order of troponin. If the latter were the correct explanation, then its contribution to the 9M cluster would amount to ~5%. In summary, if any troponin or C-protein contributions to the intensity profiles of the 3M, 6M, 9M, and 15M clusters are present, then they are sufficiently weak to be ignored.

In addition, if one postulates the presence of another structure, which at P_o has the periodicity of the myosin heads, e.g., the thick filament backbone, then one would have to assume also that this structure is invisible at rest (and somehow appears at P_o), or that it undergoes an elongation comparable to the ~~1.6% spacing increase in the

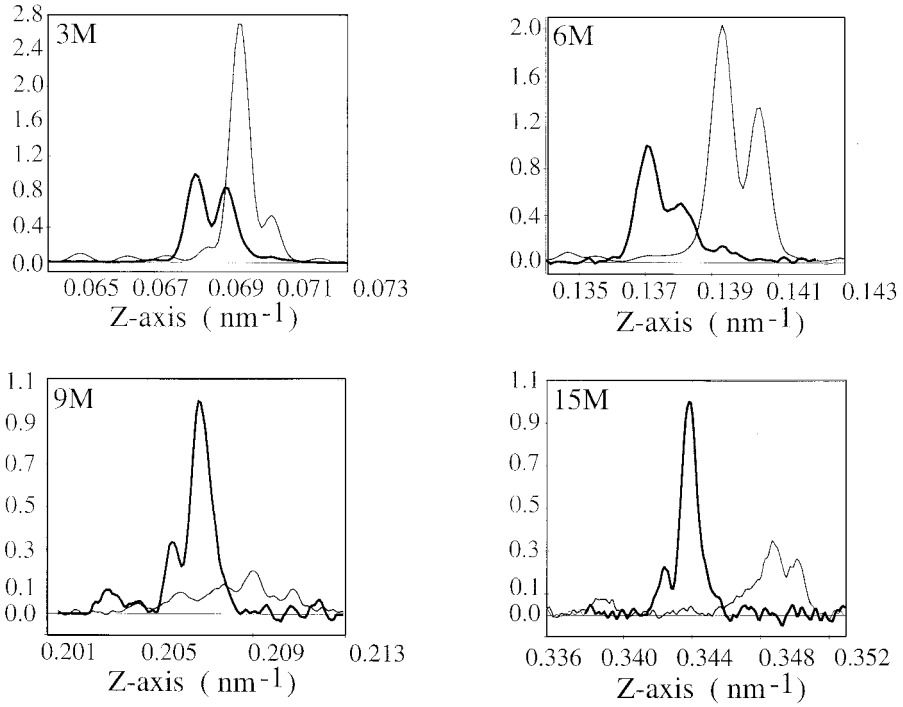

FIGURE 1 Meridional diffraction traces against the axial reciprocal space coordinate for the 3rd, 6th, 9th, and 15th myosin layer lines (labeled 3M, 6M, 9M, and 15M, respectively) at rest (*thinner lines*) and P_o (*thicker lines*). These traces are the average of six data sets obtained with the 9.775-m long camera. The P_o traces have been background subtracted and scaled between a minimum value of zero and a maximum value of one. The rest traces have been scaled so that the ratio of total integrated intensity in each cluster and that of the corresponding cluster at P_o is as determined from the total integrated intensity in the central peak of the layer line (see Results; Table 1). Note that there is very little rest intensity where the P_o clusters appear and that their center of gravity is at a spacing ~1.6% longer than at rest.

axial rise of the myosin heads. This makes it unlikely that there is a backbone contribution to the myosin clusters at P_o. In fact, it is difficult to imagine that the backbone could elongate by ~1.6% during the transition from rest to P_o given that the compliance of the thick filament is very small (Ford et al., 1981). Finally, if somehow there were a structure at P_o whose axial repeat coincided with, or was very close to, that of the myosin heads, then its contribution would be carried through the analysis we develop below and it would appear in the electron density maps (see Discussion).

Given the above considerations, we proceed from here as if the 3M, 6M, 9M, and 15M clusters at P_o are entirely due to the axial disposition of the myosin heads.

Myosin meridional clusters at P_o

A statistical analysis of the spacing of the various major peaks obtained from P_o patterns of individual muscles is given in the second column of Table 2. One finds from these that the reciprocal separations between the peaks in each cluster correspond to real-space distances of 1.00 ± 0.07, 0.95 ± 0.05, and 0.81 ± 0.13 μm for the 3M, 6M, and 9M, respectively. The statistics were not good enough to work out the corresponding distance for the 15M cluster because the spacing of the ~2.921-nm peak (Table 2) could be determined only from the averaged 15M trace (Figs. 1 and 4). This yields a value of ~0.7 μm. Despite the fact that the errors in these real-space distances are sufficiently large to make the values overlap, we note that there is a tendency in the mean value to decrease with increasing order number. The significance of this is expanded upon below.

Considerations on interference effects at P_o

To a first approximation, the low-resolution structure of the sarcomere may be regarded as two sets of myosin diffraction units symmetrically disposed on either side of the M-line. The distance between the centers of these units (i.e., the interference distance) is given by

$$L = B + (N - 1)c \quad (1)$$

where B is the length of the bare zone (~150 nm), N is the number of crown levels in each unit (~50; Squire, 1981),

TABLE 2 Spacings, relative intensities, structure amplitudes, and relative weights

Myosin orders	Spacings (nm)	Relative intensity	Structure amplitude	Relative weights
3M	14.433 ± 0.019	1.000	1.000	0.45
	14.646 ± 0.010			0.55
6M	7.183 ± 0.012	0.141	0.375	
	7.240 ± 0.007			0.33
	7.296 ± 0.006			0.67
9M	4.840 ± 0.003	0.027	0.163	0.76
	4.870 ± 0.004			0.24
15M	2.908 ± 0.001	0.014	0.117	0.84
	2.921 ± ?			0.16

Spacings and standard deviations of the major interference peaks in the myosin meridional reflections at P_o are shown in the second column, their relative intensities in the third column, relative structure amplitudes in the fourth column, and relative weights of the interference peaks in each order in the fifth column. The spacings of the 3M and 6M were obtained by combining data from two camera lengths (see Materials and Methods) and from a total of 19 muscles. Data for the 9M and 15M could be obtained only with the longest camera from a total of six muscles.

and c is their axial repeat of ~14.5 nm. Classical diffraction theory of two identical diffraction units (see Appendix) shows that if the disposition of myosin heads is sufficiently ordered to give rise to interference effects between them, then the diffracted intensities $I(Z)$ are proportional to

$$F_M^2(Z)\cos^2(\pi LZ)\,\frac{\sin^2(\pi NcZ)}{\sin^2(\pi cZ)}, \qquad (2)$$

*W*here Z is the meridional coordinate in diffraction space, $F_M(Z)$ is the meridional structure amplitude of the repeating motif, $\cos^2(\pi LZ)$ is the interference function between the two diffraction units and $\sin^2(\pi NcZ)/\sin^2(\pi cZ)$ is the Laue function accounting for the lattice of each diffraction unit (Vainshtein, 1966). Although c is due to the mass projection of three pairs of myosin heads in each crown, we assume that the mass projection of each is identical; therefore, for our purposes the repeating unit is one pair.

Similar considerations can be used concerning interference phenomena across the Z-line. However, these will not be dealt with here, as it is unlikely there is enough register between the myosin diffracting units across the Z-line to produce interference effects. This is because there is always some variability around the mean sarcomere length. The myosin heads are tethered to the thick filaments and through them to the M-line. Therefore, small variations in sarcomere lengths are sufficient to alter the phase relationships needed to produce interference effects. On the other hand, and precisely because the myosin heads are tethered to the thick filament backbone, one expects interference effects across the M-line to be significant.

Apparent interference distance and number of crown levels of myosin heads

The present results confirm that the 3M is split into a cluster of peaks (Bordas et al., 1995), and in addition, they show that the 6M, 9M, and 15M are also so. The excellent angular resolution that can be achieved unambiguously allows us to assign the origin of the peaks in each cluster to interference effects. This is because the axial width of the peaks is far too narrow to arise from the only ~50 myosin crown levels contained in each myosin diffraction unit and because the separation of the peaks in all clusters corresponds to orders of an interference distance in the range 700-1000 nm (i.e., in the range expected for the interference distance; see Eq. 1). Thus, one has to conclude that the observed clusters are due to interference effects between diffraction units symmetrically disposed on either side of the M-line.

During the course of these experiments the sarcomere length was set at 2.3 μm or somewhat less (i.e., full overlap) by measuring the rest length and, in addition, by checking out that tension response was maximal. Despite this, there is the possibility that some sarcomeres were somewhat longer (also some shorter to yield a mean sarcomere length of 2.3 μm) than the mean value. Because of this there may have been some variability in the fraction of myosin heads attached to actin at P_o. If that was the case, and assuming that the myosin heads have a different periodicity and conformation in the overlap and non-overlap regions, then the question arises as to how much of an effect this could have on the phase relationships required to set up interference effects. That these effects could not be very significant is testified by the remarkable reproducibility of interference effects in different muscles (Table 2). Nevertheless, we tested the situation by studying the behavior of the diffraction diagram when the sarcomere length was moderately increased (i.e., sarcomere lengths were kept shorter than needed to reach the onset of passive tension at ~2700 nm). The outcome of these experiments was that as the mean sarcomere length increases there is a tendency to 1) apparently increase the interference distance on the 3M cluster at P_o, 2) reduce the prominence of the 3M cluster relative to the 6M, although the absolute intensity decreased in both, and 3) cancel the interference effects for the higher orders before this was noticeable for the lower ones. In addition, we found that for the longest sarcomere length we tried, i.e., ~2650 nm, one began to detect the coexistence of two clusters in the region of the 3M. The main P_o cluster appeared to have an interference distance that was ~15% longer than at full overlap, whereas a second ill-defined cluster began to develop at approximately the position of the rest spacing. The total intensity in this developing cluster was much weaker (by ~16 times) than in the main cluster.

A rigorous treatment of this situation requires a probabilistic approach. However, a phenomenological interpretation is that as the overlap decreases only the heads furthest away from the M-line can attach to actin, and therefore their effective interference distance increases. In addition, as the intensity scales as the square of the number of heads in overlap this probably explains the intensity reduction. The heads outside the overlap zone probably diffract with a different periodicity and they do not contribute to the cluster of reflections characteristic of the attached heads. Note that if the heads beyond overlap had the same periodicity, then the interference length would not change (in fact, preliminary data from activated semitendinosus muscles brought beyond overlap indicates that in this situation the spacing of the myosin heads is close to that at rest). Thus, the contribution of the heads outside the overlap zone will occur at a different position, and it will be practically negligible unless they are a substantial fraction of the total.

In the case of a relatively small fraction of the total number of heads being outside the overlap region, it is straightforward to show that interference effects will show up as orders of a mean interference distance $\langle L\rangle$ given by

$$\langle L\rangle = B + (N-1)c + (\langle f\rangle N - 1)\Delta c, \qquad (3)$$

where $\langle f \rangle$ is the mean fraction of heads outside the overlap zone and Δc is the difference between the periodicities of the myosin heads inside and outside the overlap zone. Naturally, the $F_M(Z)$ meridional structure amplitudes will be different for both categories of heads and the Laue interference function will no longer be as given in Eq. 2. In any case, given the values of N (~50) and c (~14.54 and 14.32 nm in the overlap and non-overlap regions, respectively), Eq. 3 shows that $\langle f \rangle$ would have to be quite substantial to significantly modify the interference distance that applies at full overlap. Therefore, for practical purposes these effects may be neglected.

In practice, we found that the diffraction profiles of the 3M, 6M, 9M, and 15M can be reproduced by applying Eq. 2, where the differences between the observed and calculated profiles for each order can be minimized using N and L as floating parameters. We allowed L and N to vary while imposing the condition that B, calculated according to Eq. 1, remained in the range 150–160 nm. This minimization yielded modeled cluster profiles (not shown) similar in quality to those shown in Fig. 4. The data in Fig. 2 *A* show the values of the interference distance thus obtained for the different orders for residuals $R \leq 1.5$ times those obtained in the best fits (shown by the closed symbols in Fig. 2). The best fits were obtained for L values of 850.64/865.2, 810.02/824.58, 721.54/736.06, and 561.39/575.93 nm and N values of 49/50, 46/47, 40/41, and 29/30 for the 3M, 6M, 9M, and 15M clusters, respectively. The values of N found in the fits are correlated with those found for L (Fig. 2 *B*). Note that the values of N and L obtained from this minimization decrease with increasing order number, and we note that this decrease is independent of the values chosen for B. Obviously, N and L cannot depend on the order number, and because of this, we will from now on refer to the values of N and L that vary with the order number as apparent.

We would like to point out that the apparent values of N and L derived above are far too large (with the possible exclusion of L-apparent for the 15M) to be compatible with those expected from C-protein, where N is expected to be 7–11 and L is ~700 nm (Squire, 1981; Squire et al., 1982). This suggests once more that the contribution of C-protein to these interference phenomena is likely to be negligible. Also, the values of L are too short to be explained by having many filaments beyond the overlap zone (the data in any case are not compatible with the absence of the other features expected in this situation, e.g., the developing cluster in the region of the 3M at rest).

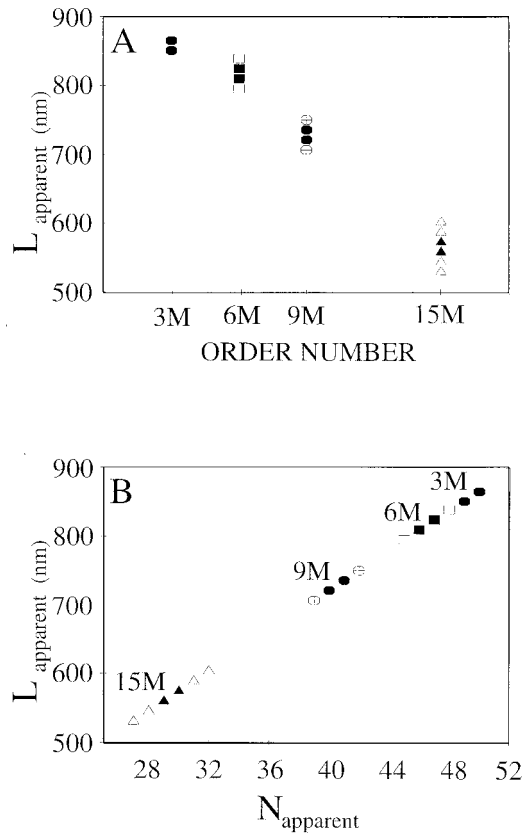

FIGURE 2 (*A*) Apparent interference distances obtained by fitting the axial profiles shown in Figs. 1 and 4 using Eq. 2 (see text) against order number. The closed symbols correspond to the best minimizations; the open symbols correspond to fits where the residuals were ≤1.5 times those of the best fits. (*B*) Apparent interference distance against the apparent value of the number of repeats needed to minimize the data shown in Fig. 1. The meaning of the symbols is as above.

Intensities of the 3M, 6M, 9M, and 15M at P_o

Fiber orientational disorder results in a progressive radial broadening (and arching) of the meridional maxima. This is clearly visible in the two-dimensional diagrams (not shown) and in the radial traces of the 3rd, 6th, 9th, and 15th myosin layer lines (Fig. 3). Note that the radial widths of the central maxima increase with the layer line index, an effect that, at least partly, is due to the angular disorder in the alignment of the filaments. No crystallographic sampling is observed in any of the layer lines.

To obtain the meridional relative intensities between the various orders while compensating for the effect of orientational disorder we have integrated the intensities under the central maximum of each layer line. The relative meridional intensities of the 3M, 6M, 9M, and 15M clusters (normalized to the respective meridional intensity of the 3M) thus derived are given in the third column of Table 2. The fourth column in Table 2 provides the meridional structure amplitudes normalized to that of the 3M. Finally, the fifth column in Table 2 gives the relative weight of each of the major peaks in the meridional clusters. These data were derived as described elsewhere (Bordas et al., 1999) by peak stripping their contributions.

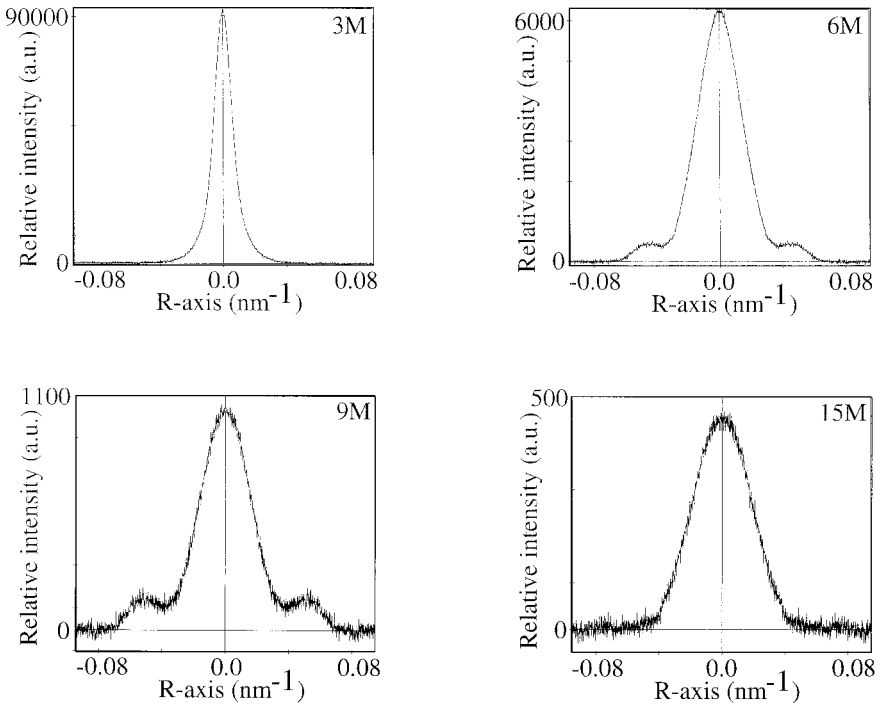

FIGURE 3 Intensities of the 3M, 6M, 9M, and 15M myosin layer lines against the radial reciprocal space coordinate. These traces were obtained by axial integration after background subtraction of the regions containing the whole of the 3M, 6M, 9M, and 15M clusters at P_o shown in Fig. 1.

Theoretical

The interference length and the axial rise of the myosin heads derived from the 3M

Eq. 2 shows that for the two main peaks in the 3M cluster to have approximately equal relative weights (Table 2, fifth column) it is necessary that L be close to an odd multiple of $c/2$. Also, it is necessary that the value of c is nearly equal to the mean spacing of the two peaks, i.e., ~14.54 nm (Table 2, second column). Considering that the bare zone (B) is ~150 nm and N is ~50, the interference distance L must have an approximate value of $[150 + (50 - 1) \times 14.54]$ nm = 862.46 nm.

We find that 862.46/(14.54/2) = 118.55, i.e., the nearest odd multiple is 119, and consequently, L becomes ~$119 \times (14.54/2)$ nm = 865.13 nm. This value is close to that arrived at above for the 3M cluster by minimization of the classical interference formula. On the other hand, we have shown that similar minimization for the higher orders leads to lower apparent values of L (and also N). This is due to the presence of more than one periodicity or a spread of periodicities (see below for further details), but at the relatively low resolution of the 3M the apparent decrease of L and N due to these effects is small enough to be negligible.

The classical interference formula does not account for the experimental observations

The fact that the apparent values of L and N are needed to fit the data shows that the classical interference formula is inadequate to reproduce the experimental findings. Moreover, the 3M shows two major interference maxima with nearly the same weight (Figs. 1 and 4; Table 2). In this situation Eq. 2 predicts that the relative weights of the interference peaks in the 3M should be very similar to those in the 9M and 15M. On the other hand the 6M should be characterized by one intense central peak with much weaker subsidiary maxima on either side of it. This is because the minimum in the interference function should approximately coincide with the maximum of the Laue function for all the odd order reflections, whereas its maximum should coincide with that of the Laue function for all the even orders. None of these expected predictions are satisfied by the experimental observations.

Interference effects between two mirror symmetrical structures

The reason the classical interference function cannot account for the relative intensities of the peaks in the diffraction clusters is because it is assumed in its derivation that the two diffraction units are identical. However, as there is polarity between structures on either side of the M-line, the mass projections of the two diffraction units must be the mirror image of each other. Therefore, the intensity formula derived in the Appendix is the more appropriate one. This formula gives the meridional intensity as

$$I(Z) \alpha F_M^2(Z) \cos^2[\pi LZ + \phi(Z)] \left[\frac{\sin(\pi NcZ)}{\sin(\pi cZ)}\right]^2, \quad (4)$$

where $\phi(Z)$ is the phase of the repeating motif. Eq. 4 leads to the key point that the relative intensities of the peaks in a given cluster depend critically on the value of the phase.

A point to note here is that if due to uncontrolled variations in sarcomere lengths (see above), there was a significant number of heads outside the overlap zone, then the interference length in Eq. 4 would be that given by Eq. 3. The net effect would be to add a constant phase shift to all the diffraction orders. Therefore, even if the fraction of heads outside the overlap zone was substantial, Eq. 4 can still be used to obtain phase information.

Phases

In the use of Eq. 4 one can arbitrarily place the phase origin at the 3M; i.e., we assume $\phi = 0$ at this position. Note that from the point of view of constructing electron density maps (see below) what matters is not where the phase origin is, but that the same origin is used for all the diffraction orders. Then one can use the values of N, L, and c deduced from the 3M and adjust the phases until the relative weights of calculated intensities in the interference peaks agree with the experimental observations in the 6M, 9M, and 15M clusters. In doing so we found values of the phases as given in the first column of Table 3. Note that there is a phase ambiguity of 180°, because the cosine in the interference function is squared. Fourier synthesis using these phases and the intensities of the meridional Laue maxima would yield the electron density maps corresponding to the mass projection of the myosin heads if the structure were truly crystallographic.

We have found that the apparent values of N and L appear smaller/shorter with increasing order number (Fig. 2). Using 152.15 nm for B (i.e., $B = 865.1 - (50 - 1) \times 14.55$ as deduced from the N and L values appropriate for the 3M) and for the other orders the apparent values of N and L needed to minimize the line shapes with Eq. 4, one obtains phase values that are essentially identical to those derived purely by adjusting the relative intensities of the interference peaks.

TABLE 3 Phases from relative weights and peak fitting

	ϕ from relative weights (degrees)	ϕ from peak fitting (degrees)
3M	0; 180	−1.3; 178.7
6M	−103; 77	−101.0; 79.0
9M	−112; 68	−116.7; 63.3
15M	−80; 100	−75.0; 105.0

Phases were obtained from adjusting the relative intensities of the interference peaks (second column) in the myosin meridional reflections using Eq. 3, and phases were obtained from shape minimization of the intensities of the interference cluster (third column) in the myosin meridional reflections using Eq. 4.

However, it is clear that N and L must have a definite value; therefore, one must conclude that with increasing resolution the number of myosin head levels contributing in phase to the interference effect must become smaller. This cannot be explained by introducing disorder effects of either the first or the second kind (Vainshtein, 1966) in the disposition of the myosin heads. Disorder of the first kind would reduce the intensity of the Laue function without changing its half-width (i.e., contradictory to the apparent decrease of N with increasing resolution), whereas disorder of the second kind would indeed lead to an apparent decrease of the value of N with increasing order number, but not affect that of the interference distance L.

In fact, to achieve an apparent reduction of N and L with increasing resolution there has to be some spread in the periodicity c or, what in practice amounts to the same, that there is more than one periodicity. In this situation Eq. 4 can be substituted by (see Appendix)

$$I(Z)\alpha F_M^2\left[\sum_{j=-(p-1)/2}^{j=(p-1)/2} w_j\cos[\pi BZ + \pi(N-1)(c_m + j\Delta c)Z + \phi(Z)]\frac{\sin(\pi N(c_m + j\Delta c)Z)}{\sin(\pi(c_m + j\Delta c)Z)}\right]^2, \quad (5)$$

where P is the number of periodicities, the terms w_j are relative weighting factors for the various periodicities, c_m is the mean periodicity, Δc is a small periodicity increment and $F_M(Z)$ and $\phi(Z)$ are to be regarded now as the structure amplitude and phase of the average repeating motif. Minimization of the observed intensity distribution in all the clusters and that predicted by this formula yields the possible phase values. We note that one obtains essentially identical shapes whether one uses a spread of periodicities or just two periodicities. The best fit for two periodicities of equal weights is shown by the thick broken lines in Fig. 4. When a spread of periodicities with equal weights was used, then an identical result was obtained when the maximum and the minimum values of c are those of the two periodicities needed for the fit shown in Fig. 4. The phase values obtained from these fits, given in the second column of Table 3, are close to those obtained from the ratio of peak intensities (first column in Table 3). Fourier synthesis of these phases and the intensities of the meridional Laue maxima would yield the electron density maps corresponding to the average mass projection of the myosin heads.

It is not surprising that the phases obtained via fitting shapes and exact peak positions are very similar to those obtained from the more straightforward method of simply reproducing the relative weights of the peaks. This is because the introduction of a set of slightly different periodicities results in a progressive broadening of the underlying Laue interference term as well as an apparent reduction of the value of L. However, for a given phase value the

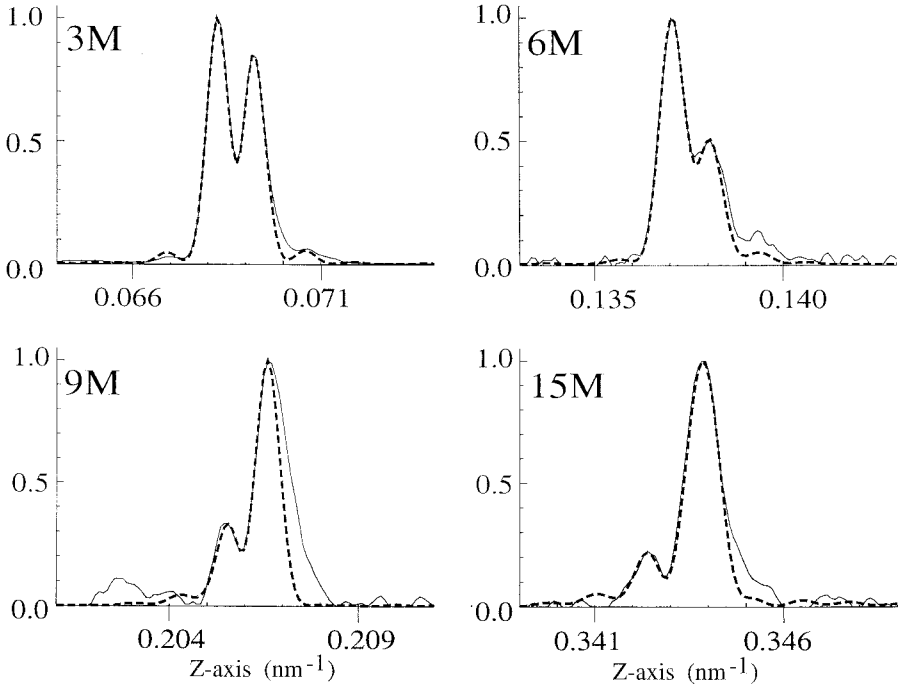

FIGURE 4 Meridional diffraction traces against the axial reciprocal space coordinates for the 3M, 6M, 9M, and 15M myosin layer lines (——; these data are the same as in Fig. 1) and fits using Eq. 4 (— — —). The fixed parameters were L = 865.1 nm; c_m = 14.55 nm; N = 50. Two periodicities were used with Δc = 0.018 nm. Because of arching of the layer lines the fits are somewhat less satisfactory on the high angle side of the clusters. The adjusted phase corrections were those given in column 2 of Table 3.

sampling of the Laue function by the interference terms closely retains the relative intensities. Therefore, the weight ratio of the resulting peaks in the splitting is practically the same as in the case of a perfect crystallographic arrangement (i.e., when Eq. 4 would apply). In fact, only in the case of a substantial width of the underlying Laue function, due to a large spread in the periodicities, the differences could be notable. In summary, from a practical point of view the extraction of phases via intensity ratios or via the additional refinement allowing shape and peak position fitting, introducing variability in the axial repeat leads to almost identical results. It is worth noting that variability in the spacing greater than 0.036 nm leads to unacceptably poor fits of the experimental results.

Possible electron density maps of the axial projections of the myosin heads

We arbitrarily define the phase origin in the center of the unit cell by assigning a phase of π, rather than zero, to the 3M. Then, given the 180° uncertainty in the phases, there are eight possible electron density maps (i.e., 2^3 combinations) that can be constructed using the relative structure amplitudes of the 3M, 6M, 9M, and 15M. The maps in the first column of Fig. 5 (corresponding to adding values of π to the smallest, i.e., negative, phases obtained for the 3M and 6M (Table 3, second column) and varying all the possible combinations of the 9M and 15M phases, are characterized by showing an asymmetric density distribution with a pronounced maximum on the left of the origin and a less prominent shoulder/maximum on its right. The second column of maps in Fig. 5 (corresponding to adding values of π and 0 to the smallest, i.e., negative, phases obtained for the 3M and 6M), and allowing all the other possible combinations for the 9M and 15M, are characterized by electron density distributions with an appearance that closely resembles the mirror image of those shown in the first column. This quasi-mirror symmetry is the inevitable consequence of the dominant values of the structure amplitudes of the 3M and 6M and their phase relationship of $\sim\pi/2$.

Obviously, each one of these maps yields a meridional diffraction diagram with intensities identical to the measured ones. Therefore, taken in isolation, their value at this stage is to show that the average mass projection of a pair of myosin heads onto the muscle axis has an asymmetric appearance. Modeling studies carried out in parallel (M. L. Bassford, 2001) show that such an asymmetry is necessary to explain the meridional intensity distribution at P_o.

DISCUSSION

The axial orientation of the myosin heads must be rigidly fixed at P_o

The results indicate that whatever the axial disposition of the myosin heads might be, their disposition must be fairly rigidly fixed so that at the resolution of the 15M the interference effects are still clearly present. Note that asynchronous motions of the myosin heads greater than about one-half our resolution limit (i.e., ~1.4 nm) would lead to the cancellation of the phase relationships between diffracting volume elements (i.e., each volume element would contrib-

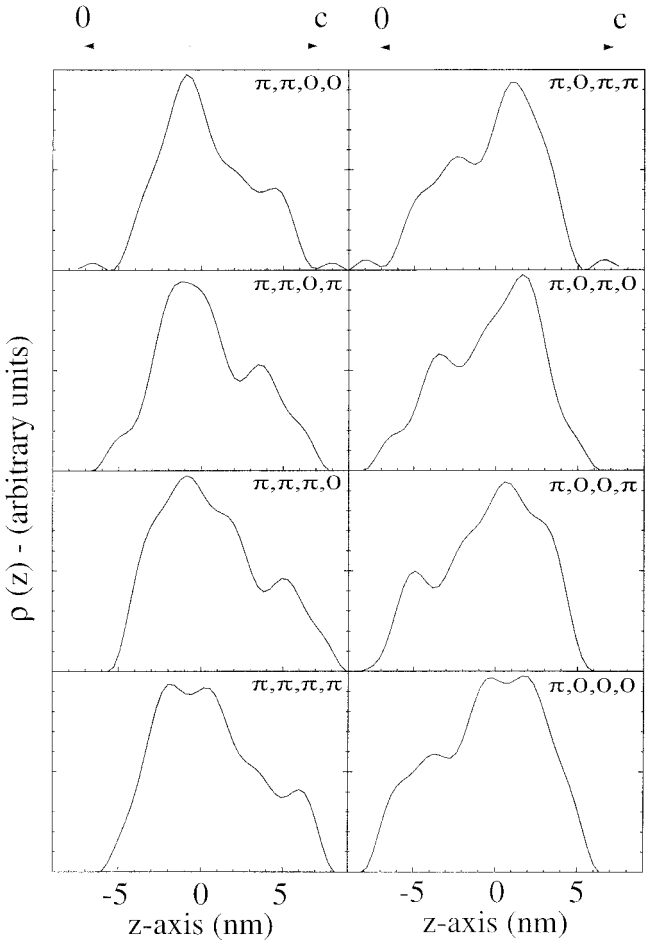

FIGURE 5 The eight possible electron density maps calculated with the phases obtained by peak fitting (Fig. 4, — — —; Table 3, column 2) are shown. The structure amplitudes used in this Fourier synthesis are listed in Table 2, column 4. Practically identical maps result by using the phases obtained from the relative weights of the peaks in each cluster (Table 3, column 1). The phase combinations are those resulting from adding the phase values given in the top right corner of each panel to the minimum (i.e., negative) phase value in Table 3 for the 3M, 6M, 9M, and 15M, respectively. The extent of the unit cell is marked by the double-headed arrow at the top of the panels. For display purposes the origin has been placed in the middle of the unit cell.

ute on average with a random phase) and the interference effect would not be expected to be more than ~1%. Moreover the Laue function would also be greatly reduced in intensity. The data (Figs. 1 and 4) show that the 15M exhibits pronounced interference phenomena; therefore, the type of pattern we have recorded could not be explained within the assumption that there are significant asynchronous axial excursions of the heads associated with the ATP cycle. Thus, the conclusion previously reached (Martin Fernandez et al., 1994) that such excursions can only be carried out either by a small fraction of the total number of heads and/or by a small portion of their mass is further reinforced by these results. In fact, as the variability in the axial repeat of the myosin heads needed to fit the experimental observation amounts to no more than 0.036 nm, the putative fraction of the heads and/or the mass undergoing such asynchronous axial excursions at P_o must be, if at all, very small indeed.

The pair of myosin heads in each crown have different mass projections

It is apparent that all the eight possible electron density maps at P_o (Fig. 5) have in common two main overlapping bands where one of them is significantly more prominent than the other. This is the consequence of the significant phase advance, or retardation, of the 6M over the 3M (Table 3), which inevitably results in the Fourier component of the latter to be split by the former into two bands of unequal intensity. As the structure amplitudes of the 3M and 6M are the dominant ones in the electron density maps, then, irrespective of the phase of the other reflections, this observation suggests that the mass projections of each head in a crown pair are different. This suggestion is reinforced by the mass projection fits described below.

Fits of calculated mass projections of pairs of myosin heads appear unique

A priori one cannot decide which one of the eight possible phase combinations (Fig. 5) might be the appropriate one. However, one can progress further by finding compatibility between the experimentally determined maps and calculated mass projections of pairs of myosin heads. To this end we have used the crystallographically determined structure of Rayment et al. (1993). We found that only the map with the π, π, 0, 0 combination of phases (top left panel in Fig. 5) could be adequately reproduced by calculated mass projection of pairs of myosin heads. The results of this fit are shown in Fig. 6, alongside the two-dimensional mass projection of the pair of myosin heads. This fit involves a pair of heads with their tail tips placed close together (~2.0 nm apart) and where one of the heads (shown by closed symbols in Fig. 6 *A*) is fairly perpendicularly orientated to the muscle axis whereas the other (gray symbols in Fig. 6 *A*) is inclined by ~33°. At the level of resolution of the electron density maps the mass projections are already sensitive to the rotation of the heads around the *y* axis (see Materials and Methods). Taking the perpendicular head as a reference, then the fitting requires that relative to it the inclined head be rotated by ~50° around its long axis. In projection this gives the inclined head an apparently straight configuration whereas the other head appears bent by ~120°. We emphasize, though, that the three-dimensional structure of both heads is identical.

We could also obtain approximate fits, although nowhere near as good, for the π, 0, π, π combination of phases by

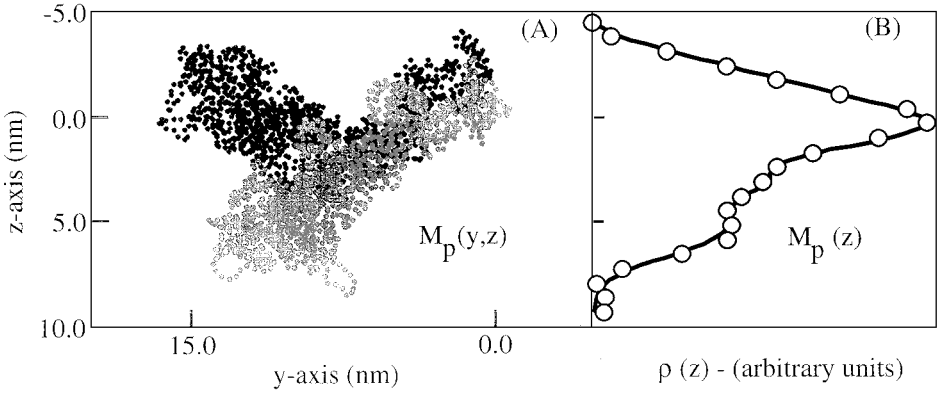

FIGURE 6 (*A*) Two-dimensional mass projection of a pair of myosin heads whose further projection onto the *z* axis yields the mass projection shown by the continuous line in *B*. Only the projections of the α-carbons in the polypeptide chain are shown. The two heads are distinguished by showing the projection of the more inclined head in gray. (*B*) Electron density map (○) constructed from adding π, π, 0, and 0 to the most negative phases obtained for the 3M, 6M, 9M, and 15M clusters, respectively (Table 3, column 2). This map, the same as that shown in the top left panel of Fig. 5, is the only one for which we could get a satisfactory fit from the mass projection of two myosin heads. The mass projection is the continuous line running through the circles.

applying a 180° rotation around the *y* axis to the disposition of myosin heads shown in Fig. 6 and giving a somewhat smaller inclination to the apparently straight head (data not shown). We failed to produce any reasonable fits for the other electron density maps. However, we note that to approximate the shape of the electron density maps it was necessary in all cases to place the two heads with different axial orientations, i.e., one head inclined and the other perpendicular to the muscle axis.

Only one of the heads in each crown pair is stereospecifically attached to actin

The disposition of the heads shown in Fig. 6 is such that if one of the heads is placed relative to the actin monomers in the thin filaments, so that it reaches the sites needed to form a specific actomyosin (AM) complex, the other head will be unable to do so because of helical and crystallographic symmetry constraints. This is valid irrespective of the position and number of contact points on the actin monomers. Therefore, the results suggest that once one of the heads in the pair forms an AM complex, the second head is unable to do so.

Previous work has shown that at P_o a first myosin layer line at a spacing of ~43.5 nm coexists with an actin-based one at a spacing of ~37.0 nm (Bordas et al., 1993). From the relative intensities of these layer lines it was concluded that ~50% of the myosin heads might be forming a stereospecific AM complex at P_o (Bordas et al., 1999). This together with the current results suggests that the 50% fraction of heads forming an AM complex arises from one of the heads in each crown pair.

The presence of a stereospecifically attached as well as a detached or nonstereospecifically attached head in the pair (note that whether detached or nonstereospecifically attached, these heads do not have to follow the thin filament symmetry) also explains why at P_o the radial maximum of the 5.9- and 5.1-nm actin layer lines does not move toward the meridian by as much as it happens in rigor (Bordas et al., 1999). This is because in rigor both myosin heads are probably forming an AM complex whereas only one does so at P_o.

Diaz-Baños et al. (1996) have calculated that the state of lowest free energy, i.e., when there is full interaction between myosin and actin forming a stereospecific AM complex, has a configuration in which the myosin head is most perpendicular to the muscle axis. Therefore, we suggest that it might be the more perpendicularly inclined head that is bound stereospecifically to actin and the one that is responsible for the untwisting undergone by the thin filament during isometric contraction (Bordas et al., 1999). We note that upon a release of ~4.0 nm/half-sarcomere the second head will be in a position where it can conveniently reach binding sites in the next actin monomers. It is attractive to speculate that the inclined head is available to take over from that forming the AM complex when the muscle is subjected to a sudden release of appropriate size so that tension can be quickly reestablished. Such a possibility has been proposed (Huxley and Tideswell, 1996) as a way to reconcile the existence of thin filament compliance (Huxley et al., 1994; Wakabayashi et al., 1994; Bordas et al., 1999) with the mechanical behavior of muscle fibers subjected to quick releases. Moreover, a structural situation such as the one shown in Fig. 6 implies that the probable reason why both heads cannot have identical positions with respect to the thin filament is that the head forming the AM complex obstructs the attachment of the other head with the same configuration. Huxley and Tideswell (1997) have developed

such a hypothesis to provide an explanation for the phenomenon of repriming (Lombardi et al., 1992). The present results provide direct structural support for this hypothesis.

Which one of the heads in the pair forms an AM complex is ambiguous at this stage

Even though for the reasons stated above, and also from time-resolved x-ray diffraction data (where the response of the interference spacing of the 3M has been followed during a quick release; unpublished data), we tend to favor the hypothesis that the more perpendicular head forms an AM complex, whereas the other one is ready to take over if/when needed. Therefore it is the population of the former type of head that is responsible for the appearance of the actin-based layer lines during isometric contraction, whereas the latter type is responsible for the remnants of myosin layer lines at P_o (Bordas et al., 1993, 1999). However, at this stage one must leave open the possibility that the actual situation may be the other way around. If indeed that was the case, we note that the inclined and now assumed attached head (Fig. 6) is reminiscent of that in rigor (Whittaker et al., 1995). The other, more perpendicularly aligned, head exhibits, on the chosen view for the projection, the $\sim 120^o$ bent configuration of the nucleotide-free myosin head (Rayment et al., 1993). However, it is conceivable that an equally good fit to the mass projection might be obtained by bending the rigor head, via a hinged movement of its tail, such as it has been proposed from analysis of crystals of myosin fragments (Holmes 1997). If this were the case, we note that the swing of the tail between the two configurations shown in Fig. 6 would be close to 10.0 nm rather than the much smaller swing of ~3.5 nm deduced from electron microscopy (Whittaker et al., 1995).

Be what it may, the point at this stage is that to interpret x-ray diffraction data from muscle tissues, during the various mechanical protocols to which they are submitted, it is important to include in the modeling that the two myosin heads may have distinctly different axial orientation at the plateau of isometric contraction.

APPENDIX

Let us assume two one-dimensional diffraction units whose centers of gravity are separated by a distance L and that each has N levels of a repeating motif, where the repeat between motifs is c. In the case of striated muscle the repeating motif is well approximated by the axial mass projection of one pair of myosin heads and L is the interference distance across the M-line. Because there is polarity across the M-line the repeating motifs in one diffraction unit are the mirror image of those in the other. Then if we let $F_{1M}(Z)e^{i\phi 1(Z)}$ be the transform of the mass projection of one pair of myosin heads and $F_{2M}(Z)e^{i\phi 2(Z)}$ be that of its mirror image, then their phases must be opposite whereas their modulus must be the same. Therefore,

$$F_{1M}(Z) = F_{2M}(Z) = F_M(Z)$$

and

$$\phi_1(Z) = -\phi_2(Z) = \phi(Z)$$

The transform of the diffraction unit on one side will be

$$F_M(Z)e^{i\phi(Z)}\frac{\sin(\pi NcZ)}{\sin(\pi cZ)}e^{i\pi(N-1)cZ},$$

where

$$\frac{\sin(\pi NcZ)}{\sin(\pi cZ)}e^{i\pi(N-1)cZ}$$

is the lattice transform or Laue function with the origin placed at the M-line (Vainshtein, 1966). The transform of the diffraction unit in the opposite side will be the above with ϕ replaced by $-\phi$.

The centers of gravity of the two diffracting units are separated by a distance $L = B + (N - 1) \times c$. To achieve this it is necessary to shift each diffraction unit by $B/2$ relative to the origin. Therefore, the total transform can be written as

$$F_M(Z)e^{i\phi(Z)}\frac{\sin(\pi NcZ)}{\sin(\pi cZ)}e^{i\pi(N-1)cZ}e^{i\pi\left(\frac{B}{2}\right)Z} + F_M(Z)e^{-i\phi(Z)}\frac{\sin(\pi NcZ)}{\sin(\pi cZ)}e^{i\pi(N-1)cZ}e^{-i\pi\left(\frac{B}{2}\right)Z}.$$

The expression above multiplied by its complex conjugate corresponds to the meridional intensities. After some manipulation one obtains

$$I(Z)\alpha F_M^2(Z)\cos^2[\pi LZ + \phi(Z)]\left[\frac{\sin(\pi NcZ)}{\sin(\pi cZ)}\right]^2.$$

The usefulness of this formula is that it shows that whenever there is an interference phenomenon between two diffraction units that are the mirror image of each other, then the ratio of intensities of the interference peaks within a given cluster, i.e., within the region where the Laue function has significant values, is very sensitive to the value of the phase of the repeating motif at this particular cluster. Naturally, if the two diffraction units are identical, then the effect of the phase cancels out in the derivation and one recovers the classical formulation of interference effects between two identical diffraction units.

Implicitly in the derivation of the formula above there is the assumption that there is a perfect crystallographic arrangement in the axial disposition of the repeating motifs, as well as in the disposition of the diffraction units on either side of the M-line. Clearly this cannot be our case if only because the tail end of the myosin heads have to follow the axial repeat of the points at the thick filament backbone on which the heads are tethered, whereas the globular part of a fraction of the heads will be attached to the thin filament and another fraction may not be attached at all. Therefore, in practice, there may be slightly different periodicities, especially for the globular part of the head.

This above can be formally incorporated in the formulation by including a spread of spacings and replacing the structure amplitude and phase of the repeating motif by that of the mean repeating motif. Therefore, the meridional intensities may be represented by

$$I(Z)\alpha F_M^2\left[\sum_{j=-(p-1)/2}^{j=(p-1)/2} w_j\cos[\pi BZ + \pi(N-1)(c_m + j\Delta c)Z + \phi(Z)]\frac{\sin(\pi N(c_m + j\Delta c)Z)}{\sin(\pi(c_m + j\Delta c)Z)}\right]^2,$$

where p is the number of periodicities, the terms w_j are relative weighting factors for the various periodicities, c_m is the mean periodicity, and Δc is a small periodicity increment. $F_M(Z)$ and $\phi(Z)$ are to be regarded now as the structure amplitude and phase of the average repeating motif. Naturally, this formula reduces to the one above if the spread in periodicities is negligible. The first consequence of including these effects in the formulation is that the width of the Laue interference term increases with increasing resolution, i.e., equivalent to an apparent reduction of N with increasing order number. The second consequence is to apparently reduce the interference distance L with increasing resolution.

REFERENCES

Bassford, M. L. 2001. Modelling the molecular structure of muscle with comparison to x-ray diffraction data. Ph.D. thesis, University of Leicester, Leicester, UK. 190 pp.

Boesecke, P., O. Diat, and B. Rasmussen. 1995. High-brilliance beamline at the European Synchrotron Radiation Facility. *Rev. Sci. Instrum.* 66:1636–1638.

Bordas, J., G. P. Diakun, F. G. Diaz-Baños, J. E. Harries, R. A. Lewis, J. Lowy, G. R. Mant, M. L. Martin-Fernandez, and E. Towns-Andrews. 1993. Two-dimensional time-resolved x-ray diffraction studies of live isometrically contracting frog sartorius muscle. *J. Muscle Res. Cell Motil.* 14:311–324.

Bordas, J., J. Lowy, A. Svensson, J. E. Harries, G. P. Diakun, J. Gandy, C. Miles, G. R. Mant, and E. Towns-Andrews. 1995. X-ray evidence that in contracting muscle there exist two distinct populations of myosin heads. *Biophys. J.* 68:99s–105s.

Bordas, J., A. Svensson, M. Rothery, J. Lowy, G. P. Diakun, and P. Boesecke. 1999. Extensibility and symmetry of actin filaments in contracting muscles. *Biophys. J.* 77:3197–3207.

Diaz-Baños, F. G., J. Bordas, J. Lowy, and A. Svensson. 1996. Small segmental rearrangements in the myosin head can explain force generation in muscle. *Biophys. J.* 71:576–589.

Dobbie, I., M. Linari, G. Piazzesi, M. Reconditi, N. Koubassova, M. A. Ferenczi, V. Lombardi, and M. Irving. 1998. Elastic bending and active tilting of myosin heads during muscle contraction. *Nature.* 396:383–387.

Ford, L. E., A. F. Huxley, and R. M. Simmons. 1981. The relation between stiffness and filament overlap in stimulated frog muscle fibres. *J. Physiol.* 311:219–249.

Haselgrove, J. C. 1975. X-ray evidence for conformational changes in the myosin filaments of vertebrate striated muscle. *J. Mol. Biol.* 92:113–143.

Holmes, K. C. 1997. The swinging lever-arm hypothesis of muscle contraction. *Curr. Biol.* 7:R112–R118.

Huxley, H. E. 1969. The mechanism of muscular contraction. *Science.* 164:1356–1366.

Huxley, A. F. 1974. Muscular contraction. *J. Physiol.* 243:1–43.

Huxley, H. E., and W. Brown. 1967. The low-angle x-ray diagram of vertebrate striated muscle and its behaviour during contraction and rigor. *J. Mol. Biol.* 30:383–434.

Huxley, H. E., R. M. Simmons, A. R. Faruqi, M. Kress, J. Bordas, and M. H. J. Koch. 1981. Millisecond time resolved changes in x-ray reflections from contracting muscle during rapid mechanical transients, recorded using synchrotron radiation. *Proc. Natl. Acad. Sci. U.S.A.* 78:2297–2301.

Huxley, H. E., R. M. Simmons, A. R. Faruqi, M. Kress, J. Bordas, and M. H. J. Koch. 1982. Time resolved x-ray diffraction studies of the myosin layer line reflections during muscle contraction. *J. Mol. Biol.* 158:637–684.

Huxley, H. E., R. M. Simmons, A. R. Faruqi, M. Kress, J. Bordas, and M. H. J. Koch. 1983. Changes in the x-ray reflections from contracting muscle during rapid mechanical transients and their structural implications. *J. Mol. Biol.* 169:469–506.

Huxley, H. E., A. Stewart, H. Sosa, and T. Irving. 1994. X-ray diffraction measurements of the extensibility of actin and myosin filaments in contracting muscle. *Biophys. J.* 67:2411–2421.

Huxley, A. F., and S. Tideswell. 1996. Filament compliance and tension transients in muscle. *J. Muscle Res. Cell Motil.* 17:507–511.

Huxley, A. F., and S. Tideswell. 1997. Rapid regeneration of the power stroke in contracting muscle by attachment of second myosin head. *J. Muscle Res. Cell Motil.* 18:111–114.

Irving, M., V. Lombardi, G. Piazzesi, and M. A. Ferenczi. 1992. Myosin head movements are synchronous with the elementary force-generating process in muscle. *Nature.* 357:156–158.

Lombardi, V., G. Piazzesi, and M. Linari. 1992. Rapid regeneration of the actin-myosin power in contracting muscle. *Nature.* 355:638–641.

Malinchik, S. B., and V. V. Lednev. 1992. Interpretation of the x-ray diffraction pattern from relaxed skeletal muscle and modelling of the thick filament structure. *J. Muscle Res. Cell Mot.* 13:406–419.

Martin Fernandez, M. L., J. Bordas, G. P. Diakun, J. E. Harries, J. Lowy, G. R. Mant, A. Svensson, and E. Towns-Andrews. 1994. Time resolved x-ray diffraction studies of myosin head movements in live frog sartorius muscle during isometric and isotonic contractions. *J. Muscle Res. Cell Motil.* 15:319–348.

Rayment, I., W. R. Rypniewski, K. Schmidt-Bäse, R. Smith, D. R. Tomchick, M. M. Benning, D. A. Winklemann, G. Wesenberg, and H. M. Holden. 1993. Three-dimensional structure of myosin subfragment-1: a molecular motor. *Science.* 261:50–58.

Rome, E. 1972. Structural studies by x-ray diffraction of striated muscle permeated with certain ions and proteins. *Cold Spring Harbor Symp. Quant. Biol.* 37:331–339.

Rome, E., T. Hirabayashi, and S. V. Perry. 1973a. X-ray diffraction of muscle labelled with antibody to troponin-C. *Nat. New Biol.* 244: 154–155.

Rome, E., G. Offer, and F. A. Pepe. 1973b. X-ray diffraction of muscle labelled with antibody to C-protein. *Nat. New Biol.* 244:152–154.

Squire, J. M. 1981. The Structural Basis of Muscular Contraction. Plenum Press, New York.

Squire, J. M., J. J. Harford, A. C. Edman, and M. Sjöström. 1982. Fine structure of the A-band in cryo-section: cross bridge distribution and the axial structure of the human C-zone. *J. Mol. Biol.* 155:467–494.

Vainshtein, B. K. 1966. Diffraction of X-rays by Chain Molecules. Elsevier, Amsterdam.

Wakabayashi, K., Y. Sugimoto, H. Tanaka, Y. Ueno, Y. Takesawa, and Y. Amemiya. 1994. X-ray evidence for the extensibility of actin and myosin filaments during muscle contraction. *Biophys. J.* 67:2422–2435.

Whittaker, M., E. M. Wilson-Kubalek, J. E. Smith, L. Faust, R. A. Milligan, and H. L. Sweeney. 1995. A 35-Å movement of smooth muscle myosin on ADP release. *Nature.* 378:748–751.